

Adsorption of CO on Rutile TiO₂ (110)-1 × 1 Surface with PreadSORBED O Adatoms

Zhuo Wang, Yan Zhao, Xuefeng Cui, Shijing Tan, Aidi Zhao, Bing Wang,* Jinlong Yang,* and J. G. Hou

Hefei National Laboratory for Physical Sciences at the Microscale, University of Science and Technology of China, Hefei, Anhui 230026, P.R. China

Received: June 27, 2010; Revised Manuscript Received: September 9, 2010

We report the investigation on the adsorption behaviors of CO on the rutile TiO₂(110)-1 × 1 surface with preadsorbed O adatoms using scanning tunneling microscopy (STM) joint with density functional theory (DFT) calculations. The STM experimental results show that the diffusive CO molecules tend to adsorb at the site close to the O adatoms, forming CO–O and CO–O–CO complexes. These complexes are quite stable against the high bias voltages and UV illumination. DFT calculations give an activation energy barrier of 0.56 eV for CO oxidation through the CO–O complex to produce CO₂. Our experimental and theoretical results both indicate that the dissociative O₂, that is, the O adatoms on Ti⁴⁺, may not be directly responsible for the catalytic oxidation at low temperature.

1. Introduction

TiO₂, as a prototype catalytic system, has been studied for decades,^{1–6} because of its applications in photocatalysis,^{2,7} selective CO removal for fuel cells,⁸ lowering automotive emission,^{9,10} and CO photo-oxidation to CO₂.^{11,12} TiO₂ has also been used as a supporting material for metal catalysts. For example, gold nanoparticles on TiO₂ were studied for their high activity for CO oxidation at low temperatures.^{13–20} Besides the particle size and shape of the metal-particle catalysts,²¹ the behaviors of the CO and O₂ adsorbates on the support oxide surfaces may also play an important role in the catalytic reaction.^{22–26} The adsorption of oxygen species on the support surfaces represents the oxygen supply during reaction, since the available gold surface area in the catalyst is generally much smaller than the support surface area. It was suggested that for the Au catalysts supported on active materials, the dominant reaction pathway involves adsorption of a mobile, molecular oxygen species on the support, dissociation at the interface, and reaction on the gold particles and/or at the interface with CO adsorbed on the gold.²⁴ To understand the actual adsorption and reaction processes, the microscopic study with an atomic resolution will provide insight into physical and chemical mechanism involved.

It is found that O₂ adsorption may result in dissociation in two channels: (i) directly at a bridge-bonded oxygen vacancy (BBO_V), healing the vacancy, and leaving an oxygen adatom on a Ti⁴⁺ site,^{27–30} and (ii) at Ti⁴⁺ sites, leaving two O adatoms on the Ti⁴⁺ row.^{30,31} These O adatoms on Ti⁴⁺ sites have been shown to alter the chemistry of adsorbates such as water, methanol, ammonia, and acetone on the TiO₂ (110) surface.^{27,28,30,32–34} Molecular O₂ can only be weakly physisorbed on a fully oxidized TiO₂ surface at low temperatures (<80 K).^{35–37} This result indicates that the physisorbed O₂ on the TiO₂ surface is not the main contributor to the oxygen supply for the CO oxidation at elevated temperatures. Chemisorbed O₂ occurs in the presence of surface negative charge, provided by defects or through capture of photoexcited electrons, which enable molecular oxygen adsorption

as O^{2–},^{28,38,39} O₂^{2–,40–43} and O₂^{4–} species.³⁷ However, such molecular oxygen species on TiO₂ have not yet directly been observed with scanning tunneling microscopy (STM), neither at BBO_V sites nor at Ti⁴⁺ sites, though the STM technique has been proved to be sensitive on characterization of adsorbed molecules or atoms on the TiO₂ (110) surface.^{29–31,44–47} Instead, only dissociative O adatoms at Ti⁴⁺ sites have been observed by STM, even at low temperature.^{30,31,44}

Another important issue is the adsorption sites of CO. A lot of work has been done on the adsorption sites and configurations of CO on the rutile TiO₂ surface.^{35,48–52} A common idea was that the BBO_V itself acts as adsorption sites for CO.^{48,52} However, by direct STM observation, our recent work reveals that the adsorption sites for CO is preferentially the next nearest neighbored Ti⁴⁺ sites close to the BBO_V at 80 K.⁵³ This fact of CO adsorption at Ti⁴⁺ sites may provide us some hints to pursue the microscopic understanding of CO oxidation.

On the oxidation of CO on TiO₂, early work by Göpel et al. suggested that CO might oxidize with bridging oxygen of the TiO₂ surface.^{48,52} However, the work by the Yates group¹¹ suggested that CO₂ photoproduction involves the interaction of chemisorbed CO with excited α -O₂ species and the lattice oxygen in TiO₂ is not chemically involved in CO₂ formation during ultraviolet (UV) irradiation. Some theoretical efforts have also been done on the adsorption and oxidation of CO and O₂ on bare TiO₂ surface.^{54,55} The results by Wu et al.⁵⁴ showed that the oxidation of CO with molecularly adsorbed O₂ takes place at the O-vacancy site and the CO oxidation energy barrier is found to be about ~0.4 eV in calculation with the 1 × 4 supercell. Alternatively, when the adsorbed O₂ is dissociated, the resulting adatoms can undergo an Eley–Rideal (ER) mechanism, that is, oxidize incoming gas-phase CO molecules with no barrier. Pillay et al.⁵⁵ calculated the dependence of CO oxidation on the coverage of O₂, giving an overall similar barrier of 0.45 eV, but increasing with the increase of O₂ coverage.

In this paper, we focused on the behaviors of CO adsorption on the rutile TiO₂(110)-1 × 1 surface with preadsorbed O adatoms at Ti⁴⁺ sites. We found that the diffusive CO molecules tend to adsorb at the sites close to the O adatoms, forming

* E-mail: (B. W.) bwang@ustc.edu.cn; (J. Y.) jlyang@ustc.edu.cn.

CO–O and CO–O–CO complexes. These complexes are relatively stable against the illumination of UV light and the bias voltage up to +4.0 V. Combining with density functional theory (DFT) calculations, we explored the possibility of the reaction pathway for CO oxidation with O adatom on TiO₂ via a Langmuir–Hinshelwood (LH) mechanism.

2. Experimental Section

Our experiment was carried out in an Omicron ultrahigh-vacuum (UHV) low temperature STM system with a base pressure of 3×10^{-11} mbar, which has been baked out sufficiently to minimize the background water. A one side polished TiO₂(110) rutile single crystal ($10 \times 5 \times 0.5$ mm³, from Princeton Scientific) was used. The sample was treated by heating at 900 K for about 20 min with a Ta foil heater mounted on the sample holder, followed by Ar⁺ sputtering (1 keV) about 15 min for tens of cycles. The sample was then transferred into the STM cryostat, which had been precooled to 80 K. The STM measurements were performed at temperatures of 80, 100, or 120 K. A chemically etched tungsten tip was used, which was cleaned by Ar⁺ sputtering and field emission. The images were acquired at constant current mode. After checking the quality of the TiO₂ surface, we allowed the sample exposing in situ to 0.5 L (1 L = 1×10^{-6} Torr s) O₂ by keeping the sample on the STM cryostat at temperatures of 80, 100, or 120 K, and then exposing to 0.1 L of CO, respectively.

3. Theoretical Calculation Details

All calculations were performed using Vienna ab initio simulation package (VASP).^{56,57} The projector augmented wave potentials were employed to represent the interaction between ions and electrons.⁵⁸ The wave functions were expanded in the plane-wave basis up to a kinetic energy of 400 eV. Exchange correlation was described using the parametrization of Perdew, Burke, and Ernzerhof within the generalized gradient approximation(PBE-GGA),^{59–62} which has been successfully applied to the calculations of similar problems. The TiO₂(110) surface was modeled using a (6 × 2) supercell with five-trilayers (O–Ti–O) by periodically repeated slabs, separated each by a 10 Å thick vacuum layer. Brillouin zone was carried out using the Monkhorst-Pack grid of (2 × 2 × 1). During the optimizations, the upper-most three layers as well as the adsorbed molecule were allowed to relax until atom forces below 0.02 eV/Å. The climbing-image nudged elastic band method (cNEB)⁶³ was used to find the saddle points along the adiabatic minimal energy pathway through the minimization of a set of four intermediate images with the force convergence criterion of 0.04 eV/Å. Theoretical STM images were simulated by the Tersoff–Hamann formula.^{64,65}

4. Results and Discussion

Figure 1 shows the STM images of a TiO₂(110)-(1 × 1) surface before and after 0.5 L of O₂ exposure. After O₂ exposure, some BBO_V's disappear, accompanying with occurrence of some protrusions at Ti⁴⁺ sites, marked by the arrows, as shown in Figure 1a and b. This behavior is attributed to the dissociatively adsorbed O₂ molecules by healing the vacancies and leaving O adatoms on Ti⁴⁺ rows, similar to the observations reported before.^{27–30} It is observed that there are five routes for O₂ dissociation on TiO₂(110), as shown in Figure 1 c₁–c₅ and d₁–d₅. The ball models of the dissociative O₂ are also correspondingly given in Figure 1 e₁–e₅. In cases 1–3 (correspondingly shown in Figure 1 c₁–c₃, d₁–d₃, and their ball

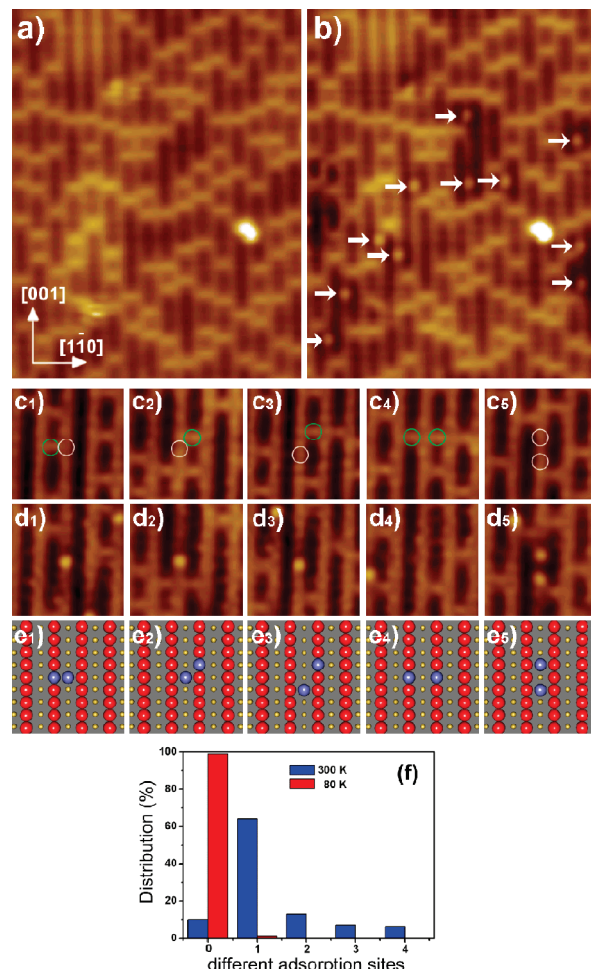


Figure 1. (a) STM image of bare TiO₂(110)-1 × 1 surface. (b) STM image within the same area after 0.5 L of O₂ exposure. The arrows mark the site of the O adatoms. Imaging conditions: 1.6 V and 0.1 nA. Size: 10.3 × 13.2 nm². (c₁–c₅) Magnified images before O₂ exposure, (d₁–d₅) magnified images after O₂ exposure, and (e₁–e₅) ball models schematically showing dissociative O₂ at BBO_V sites. The circles in c₁–c₅ depict the adsorption sites of the dissociative O₂. Images acquired at 80 K. (f) Distribution of O adatom at Ti⁴⁺ sites against the lattice distance along the Ti⁴⁺ row with respect to the original site of the opposite BBO_V.

models in e₁–e₃), each O₂ undergoes dissociation by healing one BBO_V and leaving one O adatom at the Ti⁴⁺ site close to the original position of the BBO_V. Case 1 is the most observed dissociation process at 80 K, almost with a possibility of 95%. In case 4 (Figure 1e₄), one O₂ dissociates by healing two BBO_V's simultaneously. In case 5 (Figure 1e₅), one O₂ dissociates at the Ti⁴⁺ row, exhibiting two O adatoms. The latter two cases are much rarer.

The site distributions of the O adatom at the Ti⁴⁺ obtained at 300 and 80 K have been plotted in Figure 1f. Unlike the dominant occurrence of the O adatom at the nearest Ti⁴⁺ sites to the original BBO_V sites at the low temperatures, it is observed that the O adatoms distribute to a relatively wide range far from the original BBO_V sites at room temperature. We suppose that the O₂ dissociation may still dominantly occur at BBO_V sites (as case 1 shown in Figure 1e₁); the wide range site distribution of O adatom is due to the higher diffusion rate of the O adatom on Ti⁴⁺ rows at room temperature. Using the cNEB method based on the (6 × 2) slab model, we calculated the diffusion energy barrier for the O adatom along the Ti⁴⁺ row and obtained a value of about 0.70 eV. However, this relatively high barrier

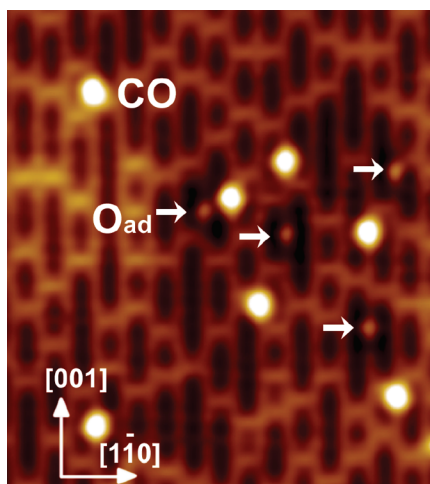


Figure 2. STM image of CO adsorption on TiO_2 with preadsorbed O adatom. The arrows mark the site of the preadsorbed O adatoms. Imaging conditions: 1.4 V and 10 pA. Size: $10.0 \times 11.2 \text{ nm}^2$, acquired at 80 K.

value indicates that the diffusion of the O adatom is difficult, especially at low temperatures, which is in agreement with our experimental observations. Though the O adatom diffusion rate can be enhanced at room temperature in some extent, it seems that the O adatoms are not an efficient oxygen supply to the metal catalytic centers.

Following the O_2 exposure, the sample was exposed to 0.1 L of CO at temperatures of 80, 100, or 120 K. As shown in Figure 2, the adsorbed CO molecules dominantly appear at the next nearest Ti^{4+} site close to the BBO_V at 80 K, as we reported before.⁵³ The apparent height of CO protrusions is much higher than that of the O adatom. At 80 K, the diffusion of the adsorbed CO and O adatom are both slow.

At elevated temperatures of 100 or 120 K, we observed that the CO molecules become diffusive, while the O adatoms keep almost immobile. As shown in Figure 3, a diffusive CO may finally find an O adatom and stick at the O adatom (see the movie in the Supporting Information), forming a complex of CO–O with a bottle-gourd-like shape. In addition, another diffusive CO may further find it and stick at the opposite side of the complex, forming another type of complex of CO–O–CO with a dumbbell shape. The CO in the complexes is much less protruded than the individually adsorbed CO (Figure 3d). In Figure 3e, the TiO_2 (110)-1 × 1 surface structure is superposed over the magnified image. It is observed that the CO and the O adatom in the complexes are adsorbed at the Ti^{4+} sites, separated by one lattice distance from each other.

The complexes of CO–O and CO–O–CO are much more immobile and stable than the individually adsorbed CO molecule. For an individually adsorbed CO, when we applied a voltage bias of about +2.6 V, the CO can be removed from the original position, and the rate is higher than 90% when we applied a voltage bias +3.0 V. In this process, the bombardment of inelastic electrons from the tip causes the CO to diffuse away or even leave from the surface. The O adatoms were difficult to be removed in this way. However, the complexes could sustain the electron bombardment with relative high energies. We just observed few events that the complexes were separated into CO and O, or the CO in complex was directly desorbed even when we applied a voltage bias up to +4.0 V. It also showed that the injection of electrons from the tip did not help to oxidize CO of the complexes. We also tried illuminating the complexes using a focused UV light (Mercury–Xenon lamp,

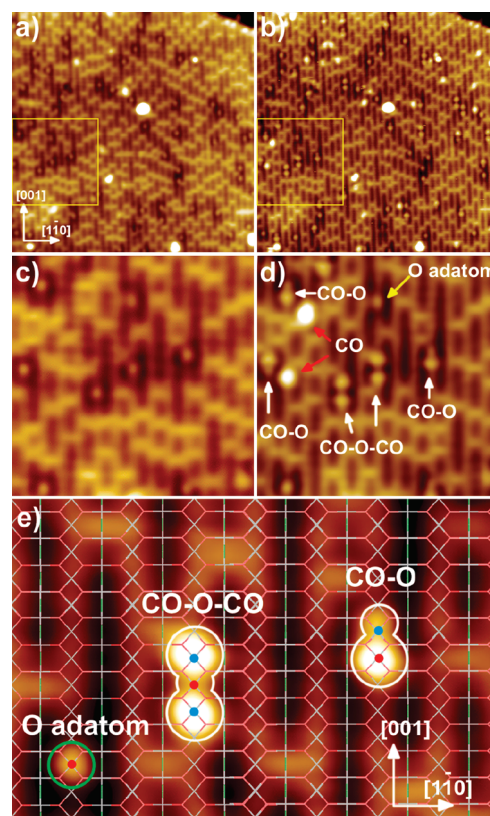


Figure 3. (a) Image of TiO_2 with preadsorbed O adatoms before exposing to CO, and (b) image of the same area as in (a) after exposing to CO (Size: $25.6 \times 25.6 \text{ nm}^2$). (c) and (d) Magnified images of the marked square in (a) and (b), respectively (Size: $9.1 \times 9.1 \text{ nm}^2$). (e) Image with superposed TiO_2 (110)-1 × 1 surface structure (Size: $5.2 \times 3.5 \text{ nm}^2$). The red dots denote the sites of the adsorbed O adatoms, and the blue dots denote the sites of the adsorbed CO. Imaging conditions: 1.4 V and 10 pA, acquired at 100 K.

200 mW power, focused spot size of about $500 \mu\text{m}$). After illumination, the bottle-gourd-like and dumbbell shapes of the complexes and their numbers remained unchanged. Hence, it indicates that such complexes are not responsible for the photocatalytic oxidation of CO, or at least, the efficiency of photocatalytic oxidation of CO from the complexes is much low.

For a better understanding of such complexes, we carried out DFT calculations and image simulations. Our previous results showed that a relatively large unit cell is important to reduce the possible interaction between the adsorbates, as well as the thickness of the slab model.^{30,53} In our DFT calculations, we used a five O–Ti–O trilayers (6×2) slab model, which contains more than 300 atoms. It has been almost to the limit of our calculation conditions. Rasmussen et al. investigated the influence of slab thickness.⁶⁶ According to their result, a four trilayers slab model is accurate enough for the calculations. Recently, Zhao et al. have checked the energy convergence of the adsorbed methanol on the rutile TiO_2 surface with different slab thicknesses up to 11-trilayers.⁶⁷ They found that the energy difference with respect to the corresponding 10-layer slab is smaller than 0.03 eV. To check the energy convergence of our DFT calculations, we tested the CO adsorption energy based on a smaller (2×1) slab model, with different slab thicknesses, where one of the surface bridging oxygens was removed. We also observed odd–even oscillation with respect to the number of trilayers, similar to that in literature.^{67,68} Our test results showed that the difference of adsorption energy is within 0.05

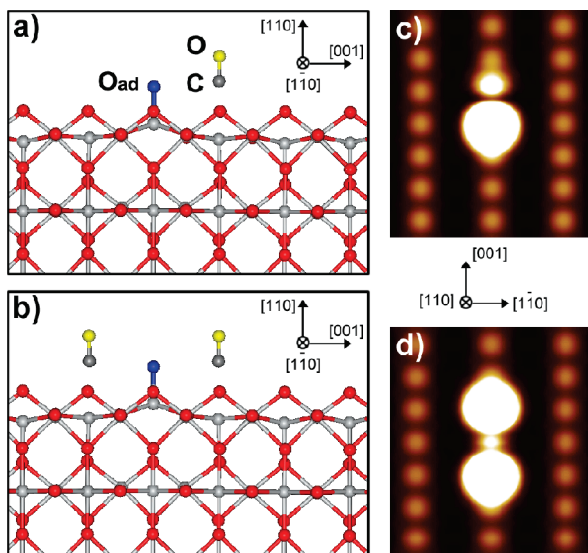


Figure 4. (a) and (b) Optimized geometries for the complexes of CO–O and CO–O–CO, respectively. (c) and (d) Simulated empty state images of the complexes of CO–O and CO–O–CO, respectively, sample bias of 1.2 V at constant height of 3.0 Å.

eV when the number of trilayers is greater than five. This is consistent with the results by Zhao et al. where the energy difference obtained for 5-trilayers and 11-trilayers are within 0.1 eV.⁶⁷ Therefore, we think our calculated results using a five-trilayers model are under a reasonable level of accuracy.

Figure 4a and b shows the geometries of the complexes using a 6 × 2 supercell with five triple-layers slab model. In the optimized configurations, the C–O bond length of CO in the complexes keeps nearly the same as that in the individually adsorbed CO. However, the distance between the C moiety of CO and the Ti atom changes from 2.50 Å for individually adsorbed CO to 2.36 Å for the CO in the complexes. This may explain the relative change of the apparent heights between the individually adsorbed CO and the CO in complexes (Figure 3d). From our calculations, it is observed that, when an O adatom adsorbs at Ti⁴⁺ site, it pulls out the Ti⁴⁺ atom from its position on a stoichiometric surface by 0.69 Å, making it higher than the in-plane-O atoms. Figure 4c and d gives the simulated images of the two types of complexes, which are in good agreement with the experimental images.

In the calculations, the diffusion barrier for CO obtained from the cNEB method is about 0.34 eV, in which the existence of the O adatom does not change the diffusion barrier too much.^{53,55} CO has the highest adsorption energy of 0.48 eV at the nearest Ti⁴⁺ site to the O adatom and is reduced to 0.40 and 0.33 eV at the Ti⁴⁺ site at the next nearest and the third nearest Ti⁴⁺ sites, respectively. The enhanced chemisorption energies near the O adatom make the CO tend to adsorb at the site close to the O adatom. This result is self-consistent with the reduced Ti–C distance in the complexes, indicating that the formation of complexes enhances the interaction between the CO and the TiO₂ substrate.

We calculated the charge density difference, as shown in Figure 5. The charge transfer between the Ti⁴⁺ atom and the O adatom is obvious, which may weaken the bond between the Ti⁴⁺ atom and the lattice O atoms and cause the Ti⁴⁺ atom to be lifted from its position on a stoichiometric surface (Figure 4). Compared to that for the individually adsorbed CO (Figure 5a), the charge density differences of CO in the complexes are obviously affected by the O adatom (Figure 5b and c). There is

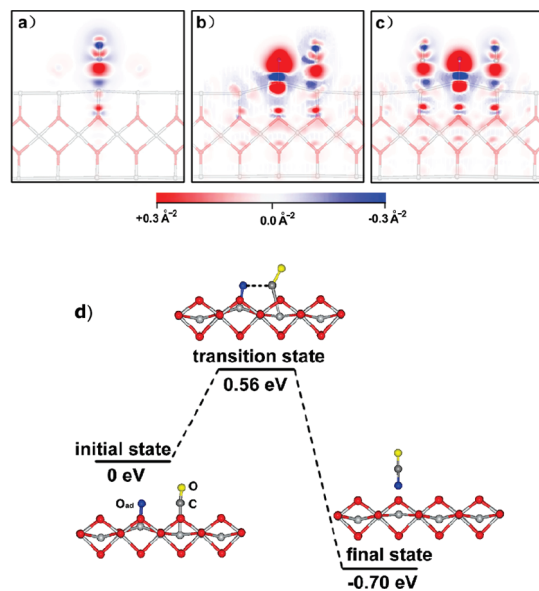


Figure 5. Charge density difference of (a) individually adsorbed CO, (b) CO–O complex, and (c) CO–O–CO complex on the TiO₂(110) surface. Differential electron density is integrated along the [110] direction. Red and blue isosurfaces represent electron gain and loss. (d) Energy profile of possible CO oxidation with the O adatom on the TiO₂ (110) surface.

charge depletion within the region between the C and O adatom, which may be attributed to the charge transfer between them, since the O adatom can get electrons due to its unoccupied bonding orbitals (p_x and p_y orbitals partially occupied). The charge accumulation between the C and Ti is slightly enhanced, reflecting the strengthened interaction between CO and the substrate.

We further examined the possible reaction pathway for CO oxidation with the O adatom on TiO₂ via the LH mechanism using the cNEB method based on the (6 × 2) with five-triple-layers slab model of TiO₂(110) surface. The configurations of molecules and the energy profile are given in Figure 5d. In the first step of the oxidation pathway, the C moiety of CO in the CO–O complex and the O adatom are drawn close to each other with the C–O distance of 1.50 Å, and the C and the O adatom become at the same height above the surface. As a result, the C–O bond forms, completing the reaction and producing CO₂. The energy barrier is about 0.56 eV.

As an approximate estimation, we may use the van't Hoff's rule: for every temperature rise of 10 °C, rate of reaction doubles, $k_{T+10}/k_T \sim 2$, where k is the reaction rate. Then, we have $k_{300}/k_{80} \sim 2^{22}$. Approximately, we adopt the value for reaction CO + O + (CO) → CO₂ + (CO) in the temperature range of 250–500 K, as the room temperature reaction rate for adsorbed CO and O, that is, $k_{300} \sim 1 \text{ s}^{-1}$.⁶⁹ The reaction time is about 1 s at 300 K; therefore, the reaction time will be 48 days at 80 K. On the other hand, according to the Arrhenius equation, $k = A\exp(-E_a/K_B T)$, where K_B is the Boltzmann's constant, we have $k_{300}/k_{80} = \exp[E_a(1/K_B T_{80} - 1/K_B T_{300})] = 2^{22}$; then, we expect an activation energy of $E_a = 0.14$ eV. By considering a much higher activation energy value of 0.56 eV from our DFT calculations, the reaction time will be much longer than the estimated time. This estimation shows that the reaction rate of CO with the preadsorbed O adatom is too low to be observed at 80 K in our experiment. Our observations of the quite stable CO–O or CO–O–CO complexes are in good agreement with our calculations.

As to the ER reaction mechanism, in the former calculation by Wu et al., it was suggested that the preadsorbed O adatom may react with the incoming gas-phase CO with no barrier.⁵⁴ Experimentally, this process may cause appearance of CO₂ product on the surface or disappearance of some O adatoms due to desorption of CO₂ product. Trying to observe such a reaction, we performed more than five runs of the experiments. In each run, we always cleaned the TiO₂ sample, followed by O₂ dosing and CO dosing, and took images within the same area, which allowed us to trace and count the number of O adatoms before and after CO dosing *in situ*. The scanning areas were typically about 20 × 20 nm², which contained about 30–100 O adatoms (as shown in Figure 3a and b). By comparing the O adatoms in each pair of images before and after CO dosing, the preadsorbed O adatoms kept either individually or in forms of CO–O or CO–O–CO complexes, while the number of O adatoms remained unchanged after CO dosing. In this way, we have traced more than 1000 O adatoms whereas we did not observe any reaction event. This fact indicates that the reaction between the O adatom and the incoming gas-phase CO is not easy. Considering the low partial pressure of CO in these UHV experiments, in which there was a low possibility for gas-phase CO molecules directly attacking the O adatoms, we had tried a high CO exposure of 20 L for the O-preadsorbed TiO₂ sample. The results are qualitatively in agreement with the results from 0.1 L of CO exposure, though the CO partial pressure is still much smaller than that in a practical catalytic reaction. We also performed calculations by drawing a gas-phase CO close to an O adatom in various distances. Even with the distance of 2.0 Å between the C moiety of CO and the O adatom, after optimization, the CO went away from the O adatom without reaction. Our experimental and theoretical results both obviously disagree with the prediction of no barrier for reaction between CO and O within the ER mechanism.

5. Conclusions

In summary, we have studied the adsorption behavior of CO on the TiO₂(110) surface with preadsorbed O adatoms using low temperature STM. It is found that the diffusive CO tends to adsorb at the site close to the O adatom at 100 and 120 K, forming CO–O and C–O–CO complexes. Such complexes are almost immobile and quite stable against the bombardment of electrons from the STM tip by applying high voltages up to +4.0 V and UV illumination. Combined with the DFT calculations, the formation of the complexes is well described. The cNEB calculation gives the reaction activation energy of 0.56 eV. It seems to suggest that the complexes are not responsible for the CO oxidation at low temperatures.

Acknowledgment. This work was supported by the NBRP (2006CB922000) and NSFC (50721091, 90921013, 10825415, 20873129), China.

Supporting Information Available: STM movie for formation of CO complexes through CO diffusion on TiO₂, adsorption energy dependence on the slab thickness for CO adsorbed on reduced TiO₂ surface. This material is available free of charge via the Internet at <http://pubs.acs.org>.

References and Notes

- Diebold, U. *Surf. Sci. Rep.* **2003**, *48*, 53.
- Linsebigler, A. L.; Lu, G. Q.; Yates, J. T. *J. Phys. Chem. Rev.* **1995**, *95*, 735.
- Bond, G. C.; Thompson, D. T. *Catal. Rev.* **1999**, *41*, 319.
- Thompson, T. L.; Yates, J. T. *Chem. Rev.* **2006**, *106*, 4428.
- Chen, Y.; Crawford, P.; Hu, P. *Catal. Lett.* **2007**, *119*, 21.
- Ganduglia-Pirovano, M. V.; Hofmann, A.; Sauer, J. *Surf. Sci. Rep.* **2007**, *62*, 219.
- Henrich, V. E.; Cox, P. A. *The Surface Science of Metal Oxides*; Cambridge University Press: Cambridge, U. K., 1994.
- Park, E. D.; Lee, D.; Lee, H. C. *Catal. Today* **2009**, *139*, 280.
- Shelef, M.; McCabe, R. W. *Catal. Today* **2000**, *62*, 35.
- Twigg, M. V. *Appl. Catal. B: Environ.* **2007**, *70*, 2.
- Linsebigler, A.; Lu, G. Q.; Yates, J. T. *J. Phys. Chem.* **1996**, *100*, 6631.
- Dai, W. X.; Chen, X.; Zheng, X. P.; Ding, Z. X.; Wang, X. X.; Liu, P.; Fu, X. Z. *Chem. Phys. Chem.* **2009**, *10*, 411.
- Haruta, M.; Kobayashi, T.; Sano, H.; Yamada, N. *Chem. Lett.* **1987**, *2*, 405.
- Arenz, M.; Landman, U.; Heiz, U. *Chem. Phys. Chem.* **2006**, *7*, 1871.
- Campbell, C. T.; Parker, S. C.; Starr, D. E. *Science* **2002**, *298*, 811.
- Meyer, R.; Lemire, C.; Shaikhutdinov, S. K.; Freund, H. *Gold Bull.* **2004**, *37*, 72.
- Valden, M.; Lai, X.; Goodman, D. W. *Science* **1998**, *281*, 1647.
- Grunwaldt, J. D.; Baiker, A. *J. Phys. Chem. B* **1999**, *103*, 1002.
- Sanchez, A.; Abbet, S.; Heiz, U.; Schneider, W. D.; Häkkinen, H.; Barnett, R. N.; Landman, U. *J. Phys. Chem. A* **1999**, *103*, 9573.
- Sanchez, R. M. T.; Ueda, A.; Tanaka, K.; Haruta, M. *J. Catal.* **1997**, *168*, 125.
- Haruta, M. The Role of IB Metals. In *Workshop on Environmental Catalysis*; Ikeda: Japan, 1995; p 153.
- Jia, C. J.; Liu, Y.; Bongard, H.; Schuth, F. *J. Am. Chem. Soc.* **2010**, *132*, 1520.
- Olea, M.; Iwasawa, Y. *Appl. Catal. A: Gen.* **2004**, *275*, 35.
- Schubert, M. M.; Hackenberg, S.; van Veen, A. C.; Muhler, M.; Plzak, V.; Behm, R. J. *J. Catal.* **2001**, *197*, 113.
- Liu, L. M.; Crawford, P.; Hu, P. *Prog. Surf. Sci.* **2009**, *84*, 155.
- Dohnálek, Z.; Lyubinetsky, I.; Rousseau, R. *Prog. Surf. Sci.* **2010**, *85*, 161.
- Epling, W. S.; Peden, C. H. F.; Henderson, M. A.; Diebold, U. *Surf. Sci.* **1998**, *413*, 333.
- Henderson, M. A.; Epling, W. S.; Perkins, C. L.; Peden, C. H. F.; Diebold, U. *J. Phys. Chem. B* **1999**, *103*, 5328.
- Wendt, S.; Schaub, R.; Matthiesen, J.; Vestergaard, E. K.; Wahlström, E.; Rasmussen, M. D.; Thoststrup, P.; Molina, L. M.; Lægsgaard, E.; Stensgaard, I.; Hammer, B.; Besenbacher, F. *Surf. Sci.* **2005**, *598*, 226.
- Cui, X. F.; Wang, B.; Wang, Z.; Huang, T.; Zhao, Y.; Yang, J. L.; Hou, J. G. *J. Chem. Phys.* **2008**, *129*, 044703.
- Wendt, S.; Sprunger, P. T.; Lira, E.; Madsen, G. K. H.; Li, Z. S.; Hansen, J. Ø.; Matthiesen, J.; Blekinge-Rasmussen, A.; Lægsgaard, E.; Hammer, B.; Besenbacher, F. *Science* **2008**, *320*, 1755.
- Henderson, M. A. *Surf. Sci.* **1996**, *355*, 151.
- Du, Y.; Deskins, N. A.; Zhang, Z.; Dohnálek, Z.; Dupuis, M.; Lyubinetsky, I. *Phys. Rev. Lett.* **2009**, *102*, 096102.
- Minato, T.; Sainoo, Y.; Kim, Y.; Kato, H. S.; Aika, K.; Kawai, M.; Zhao, J.; Petek, H.; Huang, T.; He, W.; Wang, B.; Wang, Z.; Zhao, Y.; Yang, J. L.; Hou, J. G. *J. Chem. Phys.* **2009**, *130*, 124502.
- Dohnálek, Z.; Kim, J.; Bondarchuk, O.; White, J. M.; Kay, B. D. *J. Phys. Chem. B* **2006**, *110*, 6229.
- Thompson, T. L.; Yates, J. T. *Top. Catal.* **2005**, *35*, 197.
- Kimmel, G. A.; Petrik, N. G. *Phys. Rev. Lett.* **2008**, *100*, 196102.
- Sporleider, D.; Wilson, D. P.; White, M. G. *J. Phys. Chem. C* **2009**, *113*, 13180.
- Henrich, V. E. *Prog. Surf. Sci.* **1979**, *9*, 143.
- de Lara-Castells, M. P.; Mitrushenkov, A. O.; Roncero, O.; Krause, J. L. *Isr. J. Chem.* **2005**, *45*, 59.
- Lu, G. Q.; Linsebigler, A.; Yates, J. T. *J. Phys. Chem.* **1995**, *102*, 4657.
- de Lara-Castells, M. P.; Krause, J. L. *J. Phys. Chem. Phys.* **2001**, *115*, 4798.
- de Lara-Castells, M. P.; Krause, J. L. *Chem. Phys. Lett.* **2002**, *354*, 483.
- Cui, X. F.; Wang, Z.; Tan, S. J.; Wang, B.; Yang, J. L.; Hou, J. G. *J. Phys. Chem. C* **2009**, *113*, 13204.
- Besenbacher, F.; Lauritsen, J. V.; Wendt, S. *Nano Today* **2007**, *2*, 30.
- Besenbacher, F.; Lauritsen, J. V.; Linderoth, T. R.; Lægsgaard, E.; Vang, R. T.; Wendt, S. *Surf. Sci.* **2009**, *603*, 1315.
- Bikonda, O.; Pang, C. L.; Ithnin, R.; Muryn, C. A.; Onishi, H.; Thornton, G. *Nat. Mater.* **2006**, *5*, 189.
- Göpel, W.; Rocker, G.; Feierabend, R. *Phys. Rev. B* **1983**, *28*, 3427.
- Kunat, M.; Burghaus, U. *Surf. Sci.* **2003**, *544*, 170.
- Lee, S. S.; Fan, C. Y.; Wu, T. P.; Anderson, S. L. *J. Am. Chem. Soc.* **2004**, *126*, 5682.

- (51) Rodriguez, J. A.; Ma, S.; Liu, P.; Hrbek, J.; Evans, J.; Pérez, M. *Science* **2007**, *318*, 1757.
- (52) Rocker, G.; Göpel, W. *Surf. Sci.* **1986**, *175*, L675.
- (53) Zhao, Y.; Wang, Z.; Cui, X. F.; Huang, T.; Wang, B.; Luo, Y.; Yang, J. L.; Hou, J. G. *J. Am. Chem. Soc.* **2009**, *131*, 7958.
- (54) Wu, X. Y.; Selloni, A.; Nayak, S. K. *J. Chem. Phys.* **2004**, *120*, 4512.
- (55) Pillay, D.; Hwang, G. S. *J. Chem. Phys.* **2006**, *125*, 144706.
- (56) Kresse, G.; Furthmüller, J. *Comput. Mater. Sci.* **1996**, *6*, 15.
- (57) Kresse, G.; Furthmüller, J. *Phys. Rev. B* **1996**, *54*, 11169.
- (58) Blöchl, P. E. *Phys. Rev. B* **1994**, *50*, 17953.
- (59) Kresse, G.; Hafner, J. *Phys. Rev. B* **1993**, *47*, 558.
- (60) Kresse, G.; Hafner, J. *Phys. Rev. B* **1993**, *48*, 13115.
- (61) Kresse, G.; Hafner, J. *Phys. Rev. B* **1994**, *49*, 14251.
- (62) Kresse, G.; Joubert, D. *Phys. Rev. B* **1999**, *59*, 1758.
- (63) Henkelman, G.; Uberuaga, B. P.; Jónsson, H. *J. Chem. Phys.* **2000**, *113*, 9901.
- (64) Tersoff, J.; Hamann, D. R. *Phys. Rev. B* **1985**, *31*, 805.
- (65) Tersoff, J.; Hamann, D. R. *Phys. Rev. Lett.* **1983**, *50*, 1998.
- (66) Rasmussen, M. D.; Molina, L. M.; Hammer, B. *J. Chem. Phys.* **2004**, *120*, 988.
- (67) Zhao, J.; Yang, J. L.; Petek, H. *Phys. Rev. B* **2009**, *80*, 235416.
- (68) Bates, S. P.; Kresse, G.; Gillan, M. J. *Surf. Sci.* **1997**, *385*, 386.
- (69) Westley, F. *Table of Recommended Rate Constants for Chemical Reactions Occurring in Combustion*: National Standard Reference Data System, 1980; p 46.

JP1059165